

# Finite Element Analysis of Coronal Shear Fractures of the Femoral Neck: Displacement of the Femoral Head and Effect of Osteosynthetic Implants

Yukino Mori<sup>1</sup>, Hiroaki Kijima<sup>2</sup>, Mei Terashi<sup>3</sup>, Takehiro Iwami<sup>3\*</sup>, Naohisa Miyakoshi<sup>2</sup>

<sup>1</sup>Graduate School of Advanced Healthcare Engineering, Akita University, Akita, Japan

<sup>2</sup>Department of Orthopedic Surgery, Akita University Graduate School of Medicine, Akita, Japan

<sup>3</sup>Graduate School of Engineering, Akita University Department of System Design Engineering, Akita, Japan

Email: \*iwami@gipc.akita-u.ac.jp

**How to cite this paper:** Mori, Y., Kijima, H., Terashi, M., Iwami, T. and Miyakoshi, N. (2024) Finite Element Analysis of Coronal Shear Fractures of the Femoral Neck: Displacement of the Femoral Head and Effect of Osteosynthetic Implants. *World Journal of Engineering and Technology*, 12, 651-664.

<https://doi.org/10.4236/wjet.2024.123041>

**Received:** June 28, 2024

**Accepted:** August 6, 2024

**Published:** August 9, 2024

Copyright © 2024 by author(s) and Scientific Research Publishing Inc. This work is licensed under the Creative Commons Attribution International License (CC BY 4.0).

<http://creativecommons.org/licenses/by/4.0/>



Open Access

## Abstract

Coronal shear fractures of the femoral neck (CSFF) are the most challenging to treat among proximal femur fractures, directly affecting the life expectancy of patients with osteoporosis. However, an adequate osteosynthesis method has not been elucidated yet. This study investigated the displacement direction of the femoral head fragment and its effect on the bone using finite element method. A finite element model for CSFF was developed from CT image data of a patient with osteoporosis using Mechanical Finder (ver. 11). Subsequently, finite element analyses were performed on six osteosynthesis models under maximum load applied during walking. The compressive stresses, tensile stresses, and compressive strains of each model were examined. The results suggested that the compressive and tensile stress distributions were concentrated on the anterior side of the femoral neck. Compressive strain distribution in the femoral head and neck was concentrated in four areas: at the tip of the blade or lag screw, the anteroinferior side of the blade or lag screw near the fracture site, and the upper right and lower left near the junction of the blade or lag screw and nail. Thus, the distribution of both these stresses revealed that the femoral head fragment was prone to anterior and inferior displacement. Distribution of compressive strains revealed the direction of the stress exerted by the osteosynthetic implant on the bone. The same results were observed in all osteosynthetic implants; thus, the findings could lay the foundation for developing methods for placing osteosynthetic implants less prone to displacement and the osteosynthetic implants themselves. In particular, the study provides insight into the optimal treatment of CSFF.

---

## Keywords

Finite Element Analysis, Proximal Femur Fractures, Intramedullary Fixation, Coronal Shear Fractures, Femoral Neck

---

## 1. Introduction

The incidence of proximal femur fractures has been increasing globally due to the growing older adult population [1] [2]. Treatment for these fractures depends on the location of the main fracture line, rendering accurate diagnosis clinically significant. Consequently, fracture types are classified based on the location of the main fracture line (e.g., area classification, AO classification, Garden classification, Pauwels' classification, and Nakano classification to guide appropriate treatment.

Recently, a new classification for coronal shear fractures of the femoral neck (CSFF) has been proposed. These fractures are among the most challenging to treat. CSFF refers to a basicervical fracture with coronal shear force elements near it (AO Foundation/Orthopaedic Trauma Association [AO/OTA] type 31B3) or a shear fracture in the transcervical region (AO/OTA type 31B2.3) [3].

The fracture line of a CSFF is distinct from typical femoral neck fractures as it exists in the transcervical region or under the femoral head on the anterior aspect of the femoral neck and at the base of the femoral neck on the posterior aspect. Additionally, the CSFF fracture line resembles a reversed J-shaped curve, with the fracture line at the anterior cortex near the femoral head. This unique configuration makes shear forces challenging to detect using X-ray images. The shear stress and rotational instability are expected to be high, similar to AO 31-B3, Type 2, and AO 31-B2.3, Type 1-2 in the area classification reported in previous studies [4]. Internal fixation is considered appropriate because the blood flow to the femoral head is rarely interrupted, thus preventing necrosis [3]. Consequently, intramedullary nail fixation is the first-line treatment for CSFF.

Intramedullary nail fixation for treating proximal femur fractures offers advantages such as shorter operative time, less blood loss, and good fixation for unstable fractures [5]-[7]. However, it also has disadvantages, including complications such as lag screw cut-out and secondary displacement due to excessive shear forces on the fracture surface. Patients with osteoporosis, who have sparse trabecular bone in the femoral neck, are particularly prone to complications due to insufficient fixation forces [8] [9]. Therefore, achieving strong fixation against shear forces at the fracture site is crucial. Understanding the biomechanics of CSFF is essential for selecting an effective implant for osteosynthesis. To date, no biomechanical studies on CSFF have been reported.

This study investigated the mechanism and treatment of CSFF by developing a finite element model of CSFF with osteosynthesis using six different intrame-

dullary nail implants. The finite element analysis examined the direction of femoral head displacement and the effect of the implants on the bone.

To the best of our knowledge, this is the first study to perform a finite element analysis of CSFF subjected to the maximum load of walking motion and focus on the points of concentration of compressive stresses, tensile stresses, and compressive strains.

## 2. Materials and Methods

This study was approved by the institutional review board of Akita University (IRB No. 2482), and the patients provided informed consent to participate in this study.

### 2.1. Finite Element Model

The finite element model was developed based on data from a 73-year-old patient with osteoporosis (height: 165 cm, weight: 66.2 kg) who participated in the study. The patient suffered a proximal femur fracture caused by a low-energy trauma, specifically a fall from a standing height. An orthopedic surgeon diagnosed the patient with osteoporosis. The diagnosis was further supported by quantitative CT (QCT) data, as DEXA was not used to assess bone density. **Table 1** lists the detailed bone density data obtained via QCT and from the literature [10], confirming the patient's osteoporosis.

**Table 1.** Bone mineral density measured using QCT and literature values [10] (mg/cm<sup>3</sup>).

Volume of interest	Present study	Bousson <i>et al.</i> , 2001 (QCT)	
		Hip fracture subjects (n = 47), mean (SD)	Controls (n = 60), mean (SD)
Femoral head	199.4	182.2 (44.7)	237.1 (52.3)
Femoral neck	260.1	242.5 (48.7)	291.5 (48.3)

A CT scanner (Revolution CT, GE Healthcare, Little Chalfont, USA) was used for imaging, with a slice thickness of 2.5 mm and a resolution of 512 × 512 pixels per image. The bone mineral density phantom (QRM Quality Assurance in Radiology and Medicine GmbH, Baiersdorfer, Germany) was used to scan the patient's lower extremities.

The Mechanical Finder ver. 11 (Computational Mechanics Research Center, Tokyo, Japan) bone strength analysis software was used to develop the finite element model. A three-dimensional (3D) model of the intact femur was constructed by extracting the region of interest around the cortical bone from each CT image of the unfractured lower extremity. The stacked voxels were then smoothed to create a smooth 3D femur model. The main fracture line of the CSFF was incorporated into the 3D model to replicate the fracture area. An orthopedic surgeon confirmed the fracture line's location under the femoral head in the anterior part of the femoral neck and the neck base area in the posterior

part. An osteosynthesis model was then constructed to fix the fracture (**Figure 1**) using six types of intramedullary nail implants. The implants were categorized into three groups: trochanteric fixation nail-advanced (TFNA) with a single blade (DePuy Synthes, Warsaw, IN, USA) (Group 1), Gamma 3 nail with a single lag screw (Stryker, Mahwah, NJ, USA) (Group 2), and AFFiXUS hip fracture nail with two lag screws (Zimmer Biomet, Warsaw, IN, USA) (Group 3). Further, short and long nails were used for each group (**Figure 2**).

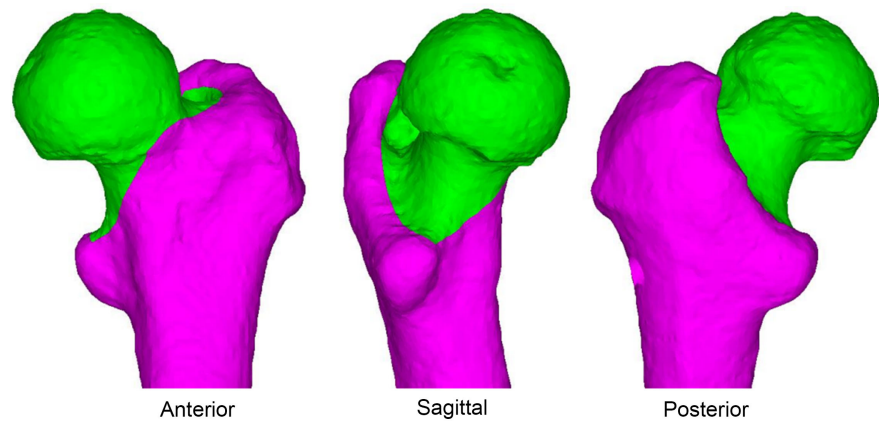


**Figure 1.** CSFF main fracture line location reproduced by a finite element model.

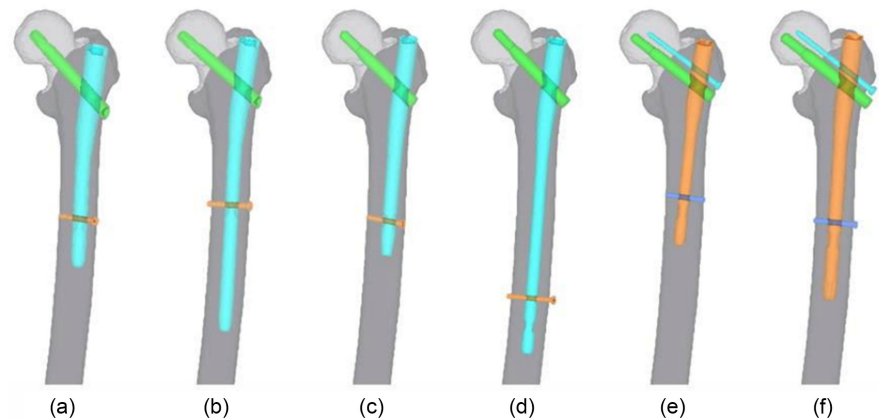


**Figure 2.** 3D models with implants inserted in CSFF: (a) short and (b) long nail of Group 1, (c) short and (d) long nail of Group 2, (e) short, and (f) long nail of Group 3.

The intramedullary nail implants had identical dimensions and were prepared following the method reported in [4]. Tetrahedral solid elements were selected, with maximum and minimum element sizes of 8 mm and 1 mm, respectively. A shell element measuring 0.3 mm in thickness was used on the outer cortical bone [11]. A mesh convergence test was performed to ensure the reliability of the analytical results. Four models were constructed with minimum mesh sizes of 0.9, 1, 2, and 3 mm. The displacement of the femoral head was evaluated under a vertical load of 1500 N, with a convergence criterion of <5% increase. The convergence criteria for CSFF were met between 2 mm and 1 mm; however, a minimum mesh size of 1 mm was chosen owing to the challenges in shaping the

screw threads at 2 mm. The average numbers of nodes, shell elements, and solid elements in the finite element model for each model were 150,930, 65,149, and 728,997, respectively.

## 2.2. Material Properties

The bone density was assigned to each element based on the Hounsfield unit (HU) values from the CT images to accurately reproduce the unique bone structure of the participant. The HU and bone density were calibrated by simultaneously imaging a bone mineral density phantom containing multiple rods with known hydroxyapatite (HA) equivalent densities,  $\rho_{HA}$ . In this study, we used the QRM-BDC/3 Phantom (QRM Quality Assurance in Radiology and Medicine GmbH, Möhrendorf, Germany). The QRM-BDC/3 contains rods with HA equivalent densities of 0, 100, and 200 mg/cm<sup>3</sup>. Using five slices of the CT data, we created a conversion formula for CT values to HA equivalent densities. This formula assigns a density value of 0 to CT values below the density of 0. The relationship between the HU values and bone density can be expressed as follows:

$$\rho = \begin{cases} 0.0(\text{HU} < -1) \\ 0.88 \times \text{HU} - 17.1(\text{HU} = -1) \end{cases} \quad (1)$$

The anisotropic material properties of the bone could not be reproduced from the HU values in the CT images when constructing the finite element model [12]. Therefore, the cancellous bone was set as isotropic in this study. The Young's modulus of the bone was estimated using the conversion formula reported in [13].

$$E = \begin{cases} 0.001(\rho = 0) \\ 33900\rho^{2.20} (0 < \rho \leq 0.27) \\ 5370\rho + 469 (0.27 < \rho < 0.6) \\ 10200\rho^{2.01} (0.6 \leq \rho) \end{cases} \quad (2)$$

The Poisson's ratio of the bone was set to 0.4 [14]. Each implant was made of titanium alloy (Ti-6Al-4V) with Young's modulus of 113.8 MPa and Poisson's ratio of 0.34; both properties were homogeneously assigned to each element [15].

## 2.3. Boundary Conditions

Each finite element model was subjected to the maximum load during gait, as calculated in [16], which served as a boundary condition (Figure 3). The loading conditions are detailed in Table 2. This value was calculated using a musculo-skeletal model to determine the muscle tension attached to the femur during locomotion and was validated against in vivo data. The displacement of the rigid body was prevented by fully constraining the six degrees of freedom of the distal femur. The coefficient of friction for bone-to-implant and bone-to-bone interactions was set to 0.3 and 0.46, respectively, based on values obtained in [17] [18].

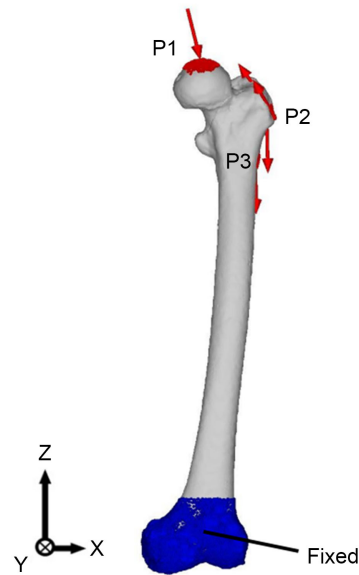


**Figure 3.** Boundary conditions.

**Table 2.** Muscular forces on proximal femur based on walking.

Force	Position	Walking		
		$F_x$ (N)	$F_y$ (N)	$F_z$ (N)
Body weight	P1	0	0	-649
Hip contact	P1	350	213	-1488
Internal resultant	P1	53	83	-508
Abductor	P2	-376	-28	561
Tensor fascia latae, proximal part	P2	-47	-75	86
Tensor fascia latae, distal part	P2	3	5	-123
Vastus lateralis	P3	6	-120	-603

This study analyzed the principal stress to predict whether the stress at the fracture site was due to compression or tension. In addition, the direction of displacement of the diaphyseal fragment was examined. The compressive strains at the total proximal femur and fracture surface were evaluated to investigate the direction of the stresses exerted by the implant on the bone.

### 3. Results

Compressive stresses were concentrated on the anterior neck side when viewed from the sagittal plane for both the femoral head and sides (**Figure 4**). Tensile and compressive stresses were concentrated on the anterior femoral neck side, but not on the femoral head side (**Figure 5**). A comparison of the mean values of compressive and tensile stresses in the femoral cross sections revealed that the tensile and compressive stresses were smaller and larger, respectively, in each group. The compressive stresses for all the osteosynthesis models ranged as 0.5 - 1 MPa, whereas the tensile stresses were less than 0.5 MPa (**Figure 6**).

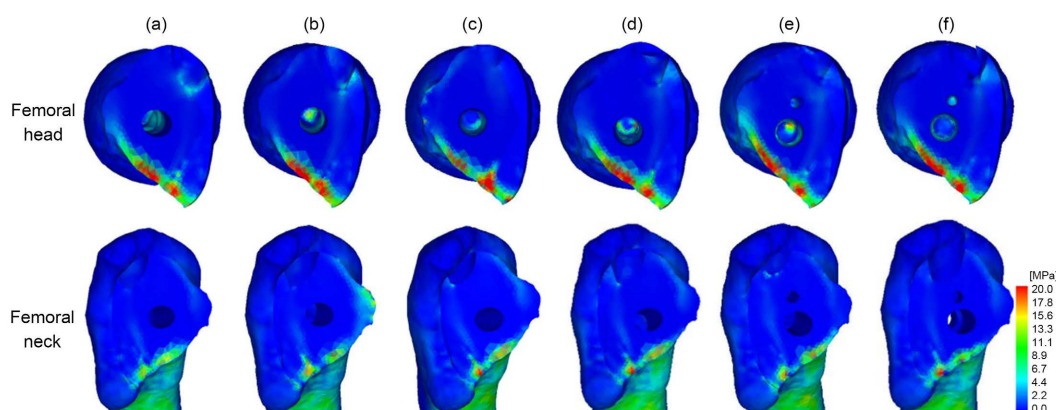


**Figure 4.** Distribution of compressive stresses at the femoral head and femoral neck.

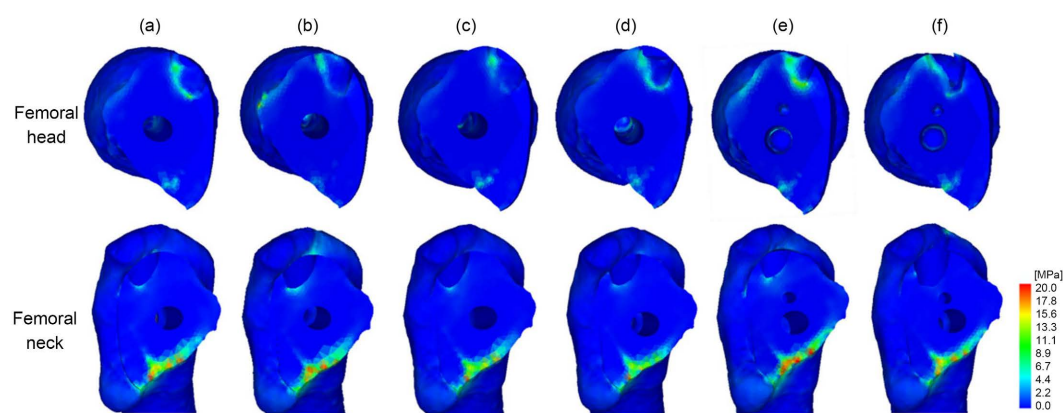


**Figure 5.** Distribution of tensile stresses at the femoral head and femoral neck.

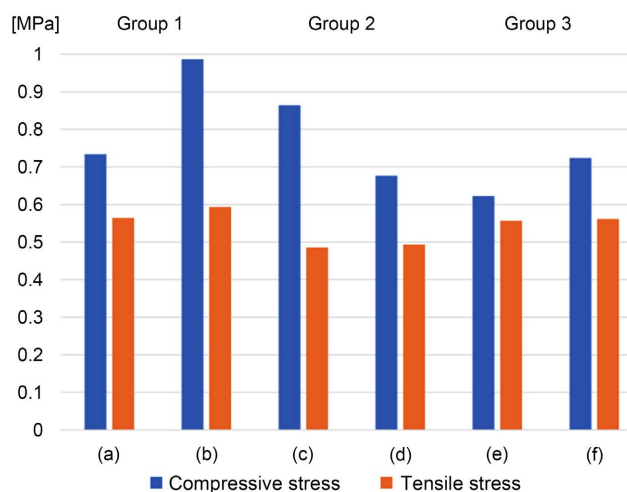


**Figure 6.** Average values of compressive and tensile stresses in the femoral cross-section.

Compressive strains in the femoral head and neck (the total proximal femur) were concentrated at the tip of the blade or lag screw, the anteroinferior side of the blade or lag screw near the fracture site, and the upper right and lower left regions near the junction of the blade or lag screw and nail (Figure 7).

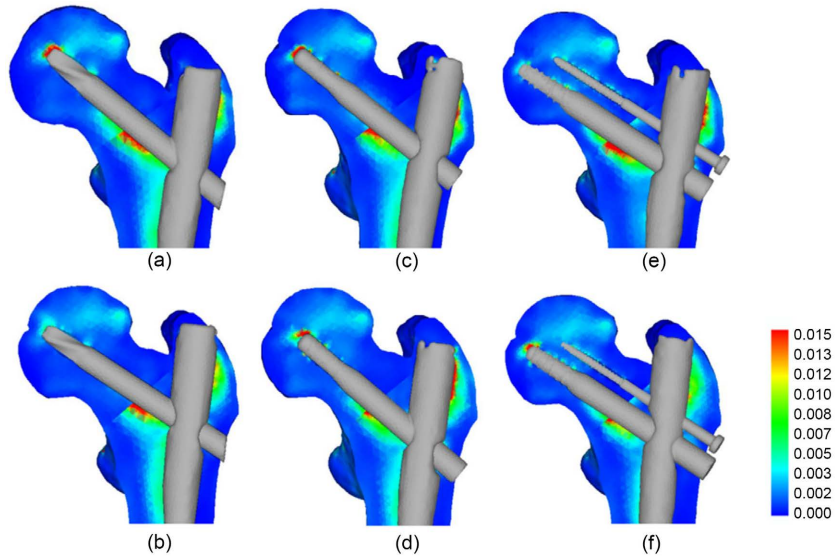


**Figure 7.** Distribution of the compressive principal strain at the fracture site in the total proximal femur.

The regions of each fracture surface were defined as illustrated in **Figure 8(i)**. The compressive strains were concentrated in the anterior region around the blade or lag screw in the femoral head lateral section and the anterior inferior region around the blade or lag screw in the femoral lateral section (**Figure 8(ii)**).

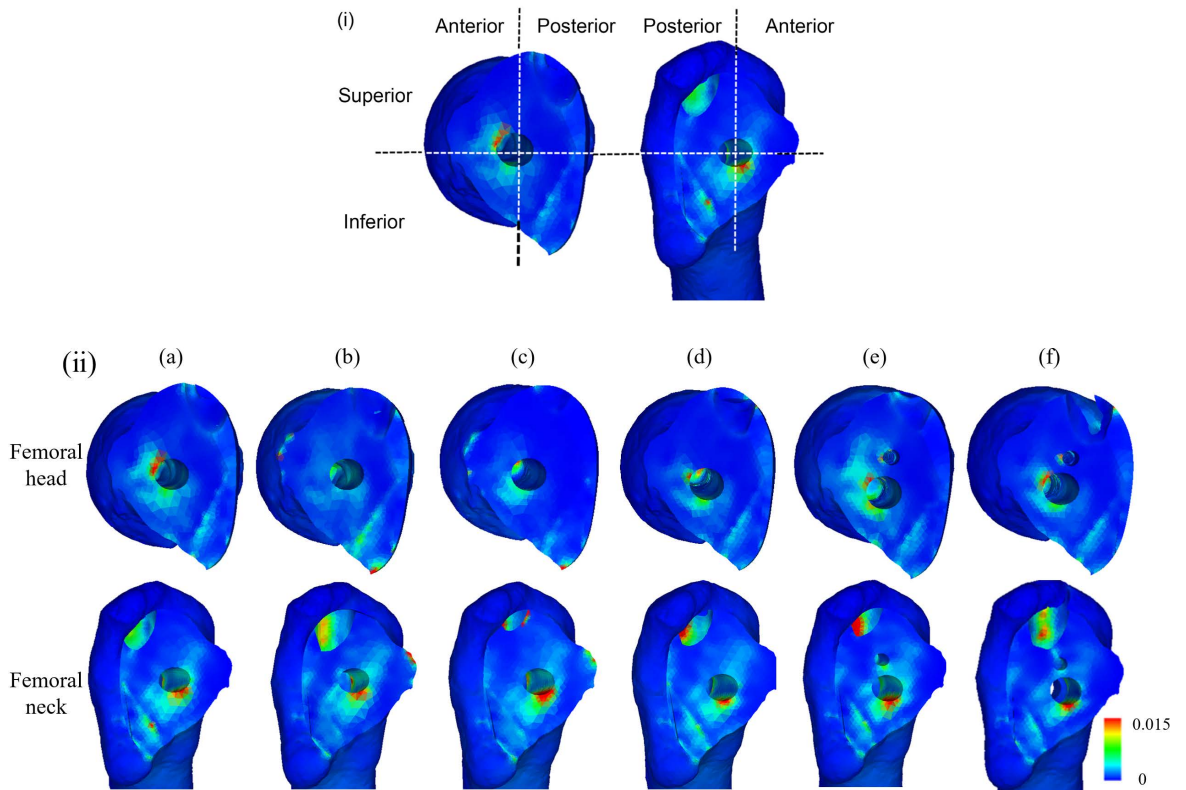


**Figure 8.** (i) Definition of the regions of the femoral head and femoral cross-section. (ii) Distribution of the compressive strain in the fracture cross-section.

All findings regarding the compressive principal stress, tensile stress, and compressive strain occurred at the same distribution positions in all osteosynthetic implants, despite the differences in the implants (**Figure 4**, **Figure 5**, **Figure 7**, and **Figure 8**).

#### 4. Discussion

To the best of our knowledge, this is the first study to demonstrate the concentration of compressive stresses at the anterior neck of the fracture cross-section on the head side, and the concentration of compressive and tensile stresses at the anterior neck on the femoral side in all models of CSFF treated with intramedullary nails. Compressive stress at the fracture site promotes fracture healing; however, excessive tensile stress could enlarge the fracture gap and even cause nonunion [19]. Our results indicate that the average compressive stresses in the femoral cross-section were higher than the tensile stresses for each group. However, tensile stress occurred at the same location as the compressive stress that promotes fracture healing, suggesting that this may hinder fracture healing. No other fracture types have been found that simultaneously concentrate compressive and tensile stresses in the same location. Therefore, CSFF is considered a specific fracture type with anterior displacement of the neck. Moreover, femoral neck fractures are more unstable when the main fracture line is vertical [20]. Considering that CSFF, including transcervical shear fractures analyzed in previous studies, has high shear stresses due to the near-vertical main fracture line [4], femoral head fragments tend to displace anteriorly and downward, highlighting the need for osteosynthesis to control displacement in this direction (**Figure 9**).

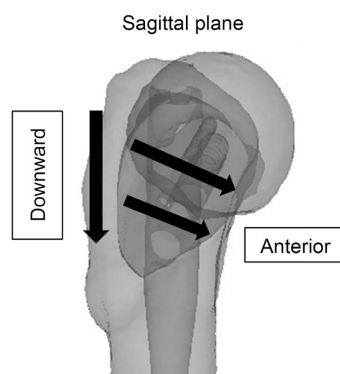


**Figure 9.** Displacement direction.

This study also revealed that compressive strains in the femoral head and neck of all models were concentrated at the tip of the blade or lag screw, the antero-inferior side of the blade or lag screw near the fracture site, and the upper right and lower left near the junction of the blade or lag screw and nail. In CSFF, the femoral head tends to displace downward on the anterior side. To resist this displacement, compressive strain was concentrated posteriorly upward at the tip of the blade or lag screw (**Figure 10** and **Figure 11**, ① and ②). The blade or lag screw, made of titanium alloy, was both elastic and rigid, thus behaving similarly

to a rigid body. This resulted in a reaction in the posteriorly upward direction, concentrating compressive strain on the anteroinferior side of the blade or lag screw near the fracture site (Figure 10 and Figure 11, ③ and ④). The stress from the blade or lag screw affects the nail in contact, leading to compressive strain around the deflected joint (Figure 10). Further, the concentration of compressive strain in the upper right near the nail joints can be attributed to the maximum load applied during walking, as illustrated in Figure 2. Therefore, compressive strain is concentrated in four areas throughout the proximal femur due to the stresses exerted by the blade, lag screw, and nail to resist displacement. The stresses caused by these osteosynthetic implants on the bone were consistent with the stress analysis at the fracture surface (Figure 12). Stress was concentrated in the anterior region due to stress ③ on the femoral head side's fracture surface. On the femoral side, stress was concentrated in the anteroinferior region around the blade or lag screw owing to stresses ③ and ④. Thus, there is a reasonable relationship between the direction of femoral head displacement and the stresses exerted on the bone by the osteosynthetic implant, implying that the model analysis adequately reproduced the actual stress environment.

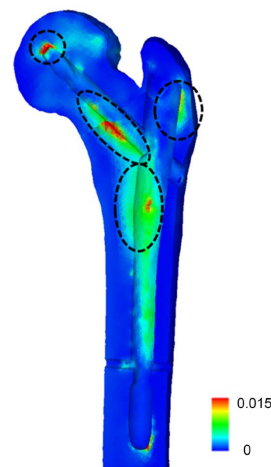


Figure 10. Distribution of compressive strain after removing the osteosynthetic implant in (a) in Figure 7.

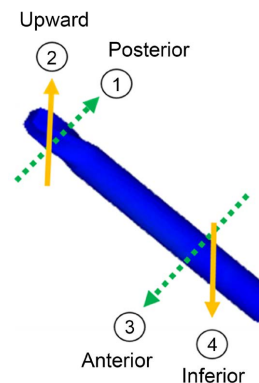
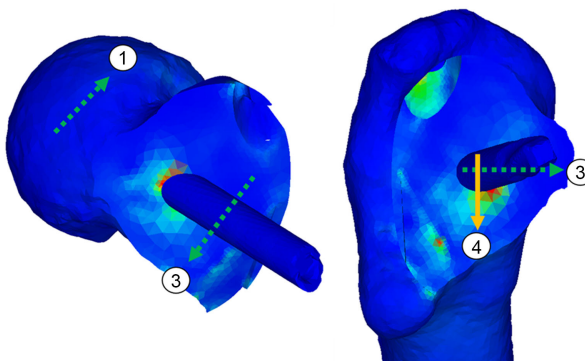


Figure 11. Stress generated on blade or lag screw.



**Figure 12.** Stress on the bone by osteosynthetic implants on the fracture cross-sections on the femoral head and femur side.

To the best of our knowledge, no biomechanical studies have previously been conducted on the mechanism and treatment of CSFF. In this study, a CSFF model treated with osteosynthetic implants was created, and finite element analysis was performed under the load condition of walking. The results showed that compressive stress, tensile stress, and compressive strain concentrated at the same location in all six osteosynthetic implant models. The analysis of compressive and tensile stresses revealed the displacement direction of the femoral head. Moreover, the analysis of compressive strains revealed that the stresses exerted on the bone by the osteosynthetic implant were consistent across all six models.

The distribution of compressive strain in CSFF differs from that in previous studies (AO 31-B3, Type 2 in area classification, and AO/OTA type 31B2.3) [4], which can be attributed to the difference in the direction of displacement. This suggests that CSFF is a new fracture type with different displacement direction and stress exertion by the implant on the bone compared to the proximal femur fractures analyzed in the literature. Therefore, the data presented in this study are expected to help develop osteosynthetic implants and methods for placing them that are less prone to displacement.

However, this study had several limitations:

- 1) The study was conducted on the bones of only one patient with osteoporosis. Therefore, studies with larger numbers of subjects are required to address the individual differences in the progression of osteoporosis, bone geometry, and bone quality.
- 2) We did not obtain data related to the existing osteosynthetic implants that could be best suited for the osteosynthesis of the CSFF in this study. This can be clarified in future studies wherein different parameters are considered.
- 3) The contact between implant components was analyzed considering fixed constraints; however, a sliding mechanism exists between the actual lag screw or blade and the nail. During surgery, the implant can be fixed in a non-sliding manner to improve fixation. In several cases, the osteosynthesis of CSFF is performed in a non-sliding manner. Another alternative is to apply pressure with a sliding mechanism to promote osteosynthesis. Therefore, a new analysis that

considers the mobility of the contact area between implant parts would be helpful.

4) In proximal femur fractures, multiple bone fragments often occur at the fracture site [21]. However, only the major fracture line was reproduced in the finite element model developed in this study. Therefore, a model that closely resembles the actual fracture treatment should be developed. Creating a model with the fracture line of each case intact would be helpful.

5) This study does not include any experimental validation of the FEA results. Complementary testing, such as actual mechanical tests, could strengthen the conclusions drawn from the simulations. Therefore, conducting mechanical testing would be beneficial.

## 5. Conclusions

In this study, we modeled CSFF, a type of proximal femur fracture, and performed finite element analysis using various implants for osteosynthesis. The femoral head fragment was found to be prone to anterior and inferior displacements. In addition, the compressive strain distribution revealed the direction of the stress exerted by the osteosynthetic implant on the bone. These results were consistent across all the different osteosynthetic implants. Therefore, the findings provide valuable insights into developing optimal treatment methods for CSFF, among the most challenging fracture types to treat.

This study is an essential step toward a more detailed and ideal analysis that requires extensive calculations. The results lay the foundation for determining the optimal treatment for CSFF, which holds great clinical significance. We hope that further studies will be conducted using the methods and results of this study and applying them to many patients.

## Ethical Statement

The study was conducted in accordance with the Declaration of Helsinki and approved by the Institutional Review Board of Akita University (IRB No. 2482).

## Conflicts of Interest

The authors declare no conflicts of interest regarding the publication of this paper.

## References

- [1] Kim, S., Moon, Y., Lim, S., Yoon, B., Min, Y., Lee, D., *et al.* (2012) Prediction of Survival, Second Fracture, and Functional Recovery Following the First Hip Fracture Surgery in Elderly Patients. *Bone*, **50**, 1343-1350. <https://doi.org/10.1016/j.bone.2012.02.633>
- [2] Dunbar, M.J., Howard, A., Bogoch, E.R., Parvizi, J. and Kreder, H.J. (2009) Orthopaedics in 2020: Predictors of Musculoskeletal Need. *The Journal of Bone and Joint Surgery-American Volume*, **91**, 2276-2286. <https://doi.org/10.2106/jbjs.h.01521>
- [3] Yamakawa, Y., Yamamoto, N., Tomita, Y., Noda, T., Inoue, T., Matsumoto, T., *et al.*

- (2022) Coronal Shear Fractures of the Femoral Neck: A Comparison with Basicervical Fractures. *European Journal of Trauma and Emergency Surgery*, **49**, 419-430. <https://doi.org/10.1007/s00068-022-02079-7>
- [4] Komatsu, M., Iwami, T., Kijima, H., Kawano, T. and Miyakoshi, N. (2022) What Is the Most Fixable Intramedullary Implant for Basicervical Fracture and Transcervical Shear Fracture?—A Finite Element Study. *Journal of Clinical Orthopaedics and Trauma*, **34**, Article ID: 102015. <https://doi.org/10.1016/j.jcot.2022.102015>
- [5] Henschel, J., Eberle, S. and Augat, P. (2016) Load Distribution between Cephalic Screws in a Dual Lag Screw Trochanteric Nail. *Journal of Orthopaedic Surgery and Research*, **11**, Article No. 41. <https://doi.org/10.1186/s13018-016-0377-y>
- [6] Zhang, Y., He, W., Liu, Y.W. and Feng, L.Z. (2015) Comparison of the Effect between Eccentric Fixation and Intramedullary Fixation for Treatment of Intertrochanteric Fractures. *China Journal of Orthopaedics and Traumatology*, **28**, 117-121.
- [7] Weiser, L., Ruppel, A.A., Nüchtern, J.V., Sellenschloh, K., Zeichen, J., Püschel, K., et al. (2015) Extra- vs. Intramedullary Treatment of Pertrochanteric Fractures: A Biomechanical *in Vitro* Study Comparing Dynamic Hip Screw and Intramedullary Nail. *Archives of Orthopaedic and Trauma Surgery*, **135**, 1101-1106. <https://doi.org/10.1007/s00402-015-2252-4>
- [8] Hollensteiner, M., Sandriesser, S., Bliven, E., von Räden, C. and Augat, P. (2019) Biomechanics of Osteoporotic Fracture Fixation. *Current Osteoporosis Reports*, **17**, 363-374. <https://doi.org/10.1007/s11914-019-00535-9>
- [9] Kouvidis, G.K., Sommers, M.B., Giannoudis, P.V., Katonis, P.G. and Bottlang, M. (2009) Comparison of Migration Behavior between Single and Dual Lag Screw Implants for Intertrochanteric Fracture Fixation. *Journal of Orthopaedic Surgery and Research*, **4**, Article No. 16. <https://doi.org/10.1186/1749-799x-4-16>
- [10] Bousson, V.D., Adams, J., Engelke, K., Aout, M., Cohen-Solal, M., Bergot, C., et al. (2010) *In Vivo* Discrimination of Hip Fracture with Quantitative Computed Tomography: Results from the Prospective European Femur Fracture Study (Effect). *Journal of Bone and Mineral Research*, **26**, 881-893. <https://doi.org/10.1002/jbmr.270>
- [11] Bessho, M., Ohnishi, I., Okazaki, H., Sato, W., Kominami, H., Matsunaga, S., et al. (2004) Prediction of the Strength and Fracture Location of the Femoral Neck by CT-Based Finite-Element Method: A Preliminary Study on Patients with Hip Fracture. *Journal of Orthopaedic Science*, **9**, 545-550. <https://doi.org/10.1007/s00776-004-0824-1>
- [12] Gómez-Benito, M.J., Garcia-Aznar, J.M. and Doblare, M. (2005) Finite Element Prediction of Proximal Femoral Fracture Patterns under Different Loads. *Journal of Biomechanical Engineering*, **127**, 9-14. <https://doi.org/10.1115/1.1835347>
- [13] Keyak, J.H., Rossi, S.A., Jones, K.A. and Skinner, H.B. (1997) Prediction of Femoral Fracture Load Using Automated Finite Element Modeling. *Journal of Biomechanics*, **31**, 125-133. [https://doi.org/10.1016/s0021-9290\(97\)00123-1](https://doi.org/10.1016/s0021-9290(97)00123-1)
- [14] Kubo, Y., Motomura, G., Utsunomiya, T., Fujii, M., Ikemura, S., Sonoda, K., et al. (2020) Distribution of Femoral Head Subchondral Fracture Site Relates to Contact Pressures, Age, and Acetabular Structure. *American Journal of Roentgenology*, **215**, 448-457. <https://doi.org/10.2214/ajr.19.21895>
- [15] Li, J., Han, L., Zhang, H., Zhao, Z., Su, X., Zhou, J., et al. (2019) Medial Sustainable Nail versus Proximal Femoral Nail Antirotation in Treating AO/OTA 31-A2.3 Fractures: Finite Element Analysis and Biomechanical Evaluation. *Injury*, **50**, 648-656. <https://doi.org/10.1016/j.injury.2019.02.008>

- [16] Heller, M.O., Bergmann, G., Kassi, J.-., Claes, L., Haas, N.P. and Duda, G.N. (2005) Determination of Muscle Loading at the Hip Joint for Use in Pre-Clinical Testing. *Journal of Biomechanics*, **38**, 1155-1163.  
<https://doi.org/10.1016/j.jbiomech.2004.05.022>
- [17] Zeng, W., Liu, Y. and Hou, X. (2020) Biomechanical Evaluation of Internal Fixation Implants for Femoral Neck Fractures: A Comparative Finite Element Analysis. *Computer Methods and Programs in Biomedicine*, **196**, Article ID: 105714.  
<https://doi.org/10.1016/j.cmpb.2020.105714>
- [18] Chen, J., Ma, J., Wang, Y., Bai, H., Sun, L., Wang, Y., et al. (2020) Correction To: Finite Element Analysis of Two Cephalomedullary Nails in Treatment of Elderly Reverse Obliquity Intertrochanteric Fractures: Zimmer Natural Nail and Proximal Femoral Nail antirotation-II. *Journal of Orthopaedic Surgery and Research*, **15**, Article No. 98. <https://doi.org/10.1186/s13018-020-01612-x>
- [19] Wu, X., Yang, M., Wu, L. and Niu, W. (2015) A Biomechanical Comparison of Two Intramedullary Implants for Subtrochanteric Fracture in Two Healing Stages: A Finite Element Analysis. *Applied Bionics and Biomechanics*, **2015**, Article ID: 475261.  
<https://doi.org/10.1155/2015/475261>
- [20] Wang, G., Tang, Y., Wu, X. and Yang, H. (2020) Finite Element Analysis of a New Plate for Pauwels Type III Femoral Neck Fractures. *Journal of International Medical Research*, **48**. <https://doi.org/10.1177/0300060520903669>
- [21] Furui, A., Terada, N. and Mito, K. (2018) Mechanical Simulation Study of Postoperative Displacement of Trochanteric Fractures Using the Finite Element Method. *Journal of Orthopaedic Surgery and Research*, **13**, Article No. 300.  
<https://doi.org/10.1186/s13018-018-1011-y>